AI-enabled Interactive Threats Detection using a Multi-camera Stereo Vision System

CONTRACT : 693JK31950002CAAP

U.S. Department of Transportation

Pipeline and Hazardous Materials Safety Administration

ASU

Project Details

CAAP Contract ID : 693JK31950002CAAP

PI : Dr Yongming Liu (yongming.liu@asu.edu)

Co-PI : Dr Yang Yu

AOR : Dr Zhongquan Zhou (Zhongquan.zhou@dot.gov)

Funding : $250,000.00

Start/End Date : 09/30/2019 – 09/29/2022

Research Award Recipient :

Arizona State University

660 S. Mill Ave.
Tempe, AZ 85281

Knowledge Transfer

Journal Papers

- Epistemic and Aleatoric Uncertainty Quantification for Defect Detection using an RGB-D Fusion Network *(In Preparation)*
- B-BACN : Bayesian Boundary-Aware Convolutional Network for Defect Segmentation *(In Preparation)*
- Semi-Supervised Surface Defect Segmentation using Activation Map Interpolation *(In Preparation)*

Source Code

- Integrated ILI Prototype : ymlasu/AI-Enabled-ILI-System-Integration
- B-BACN : Bayesian Boundary-Aware Convolutional Network for Defect Segmentation: ymlasu/Bayesian-Boundary-Aware-Convolutional-Network (github.com)
- Semi-Supervised Surface Defect Segmentation using Activation Map Interpolation: ymlasu/Semi-Supervised-Semantic-Segmentation-Activation-Map-Interpolation (github.com)

Poster presentations

- Threat Detection using Active Stereo for In-Line Inspection in Gas Pipelines, PRCI Fall Technical Meeting 2022

Doctoral Symposium

- AI-Enabled Interacting Threat Detection using a Multi-Camera Stereo-Vision System, PHM Society Conference, 2020

Project Team Acknowledgement

PI:

Dr Yongming Liu (Professor, Department of Mechanical & Aerospace Engineering, Arizona State University)

Co-PI:

Dr Yang Yu

PhD student:

Rahul Rathnakumar

Master students:

Ms. Sampriti Neog

Mr. Gowtham Dakshamoorthy

Mr. Rohith Kalyan Kavadappu

Mr. Rakesh Balamurugan

Mr. Abhishek Srinivas Loganathan

Mr. Karthikeya Vemullapalli

Mr. Chinmay Dixit

Mrs. Kailing Liu

Mr. Utkarsh Pujar

Undergraduate students:

Mr. Omar Serag

Project Management Team:

Dr. Zhouquan Zhou (PHMSA)

Mr. Robert Smith (PHMSA)

Technical Advisory and Assistance:

Ernest Lever (GTI)

Tony Lindsay (GTI)

Zoe Shall (PRCI)

Many others…

Technical Objectives

Develop	Develop software for depth extraction and pipe surface mapping using stereo-vision
Develop	Develop a hardware prototype for a vision-based inspection tool using off-the-shelf sensors
Propose	Propose accurate and efficient anomaly detection techniques
Propose	Propose physics-based models for interactive threats using FEA
Integrate	Integrate the prototype with the developed software to perform a demonstration on a pipe sample in the lab.

Educational Objectives

Training	Exposure	Teaching	Internships
Guide and train graduate students at Arizona State University for the pipe integrity assessment and risk mitigation	Integrate with existing mechanisms for undergraduate research at Arizona State University for early exposure of pipe industry research to potential engineers	Improve the current curriculum teaching at Arizona State University (MAE 598 Probabilistic methods for Engineering Analysis and Design) and using the achievement from the proposed research	Encourage the involved students to apply internships at USDOT and industry to gain practical experiences for the potential technology transfer of the developed methodologies

Executive Summary – TASK 1

Tasks	Proposed	Delivered
Task 1.1	Reports and codes for stereo vision algorithm developed for generating a depth map of pipeline surface	1. RealSense SDK is used for the baseline results in depth map generation. 2. Extremum-seeking control algorithm codes are delivered to improve depth map quality automatically.
Task 1.2	Reports and drawings for optimal design criteria and calibration procedures of the prototype device	1. Hardware calibration was performed, and design criteria were outlined for in-line inspection with a single rotating camera system.
Task 1.3	Reports and specifications for the hardware requirements for desired performance and future commercialization plans	1. Sensitivity analysis and experiments for depth camera performed and results documented. 2. Analytical analysis of depth camera to determine depth and area resolution documented and contextualized in the framework of ILI
Task 1.4	Full-scale prototype device and reports on preliminary testing in laboratory experiments	1. Proposed hardware components have been specified for the robotic platform with codes delivered. The prototype is built as a single unit and evaluated in the pipeline environment.

Executive Summary – TASK 2

Task	Proposed	Delivered
Task 2.1/Task 2.2	Reports and codes for the trained deep learning model and detection performance for pipeline anomaly detection	1. Dataset collection for ILI defect detection model. 2. Proposed a fully supervised RGB-D fusion network for semantic segmentation with MC Dropout uncertainty. 3. Proposed a point-cloud derived data stream for the CNN to leverage the geometrical features of the pipe – called the DNC representation. 4. Empirical comparison between various encoder backbones for semantic segmentation. 5. Defect quantification using semantic segmentation results for crack and corrosion defects. 6. Proposed a semi-supervised learning algorithm for defect detection based on interpolation consistency training.
Task 2.3	Reports and tools for the physics-based models developed for assessing interactive threats and damage prognostics	1. Utilized the ASME B31G and NG-18 models to estimate remaining useful life. 2. Application of a Kriging-based surrogate model trained on FEM data to estimate remaining useful life for crack and corrosion defects. 3. Interacting threat assessment for corrosion pits using FEM and comparison with ASME B31G.
Task 2.4	Reports on demonstration study of the hardware-software integrated prototype device	1. Reporting, demonstration, and code for the integrated functioning of the prototype.

Flow chart for defect detection and prognostics

Machine Learning & Image Processing Techniques

Raw data acquisition

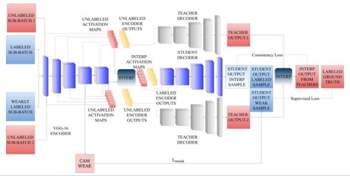

Prediction

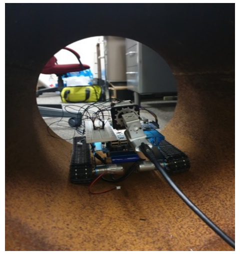

Feature extraction

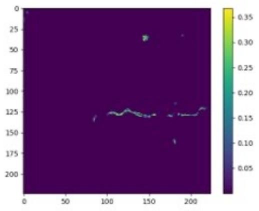

Uncertainty Quantification & risk assessment

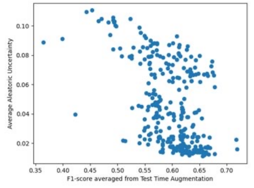

Prognostics

Analytics

Depth Map Generation using D435i

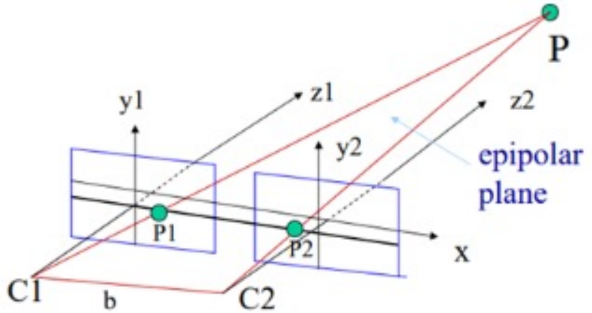

Raw depth data is acquired using "active" stere
vision: Binocular stereo + IR Dot Projection for
"fake textures"

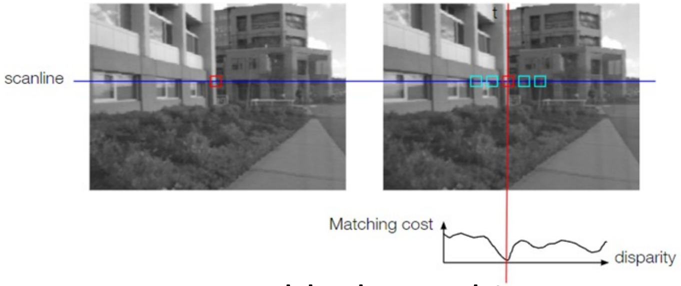

Stereo block matching

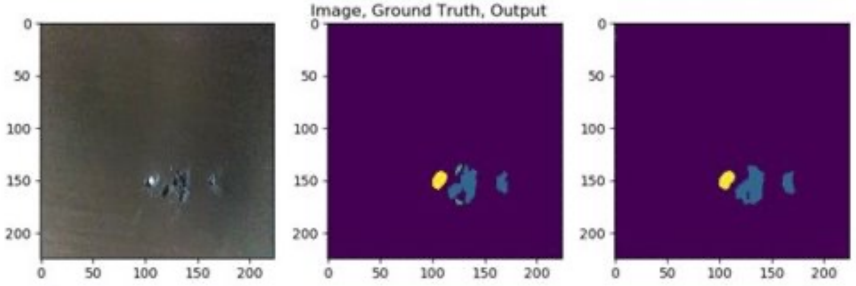

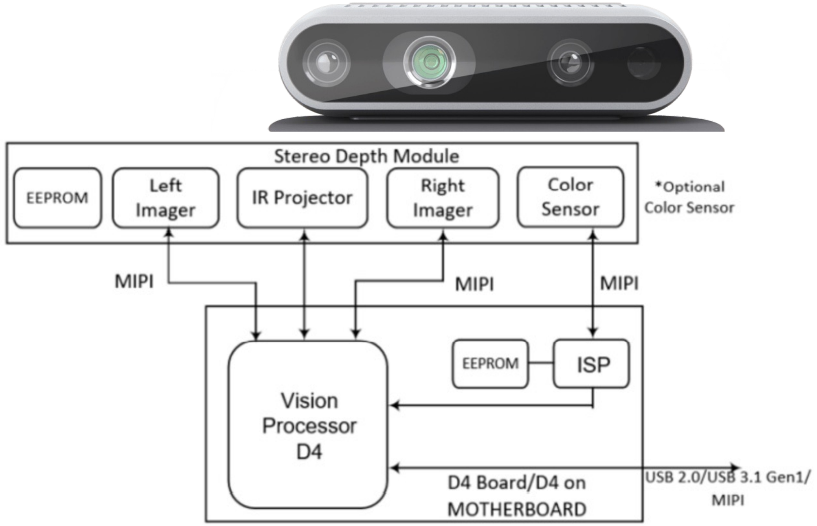

Intel Realsense ™ D435i camera system

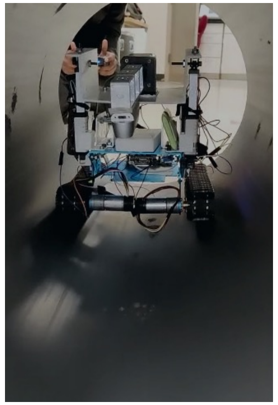

ILI system that captures pipe wall features
with 1280x720 px @ 30fps.

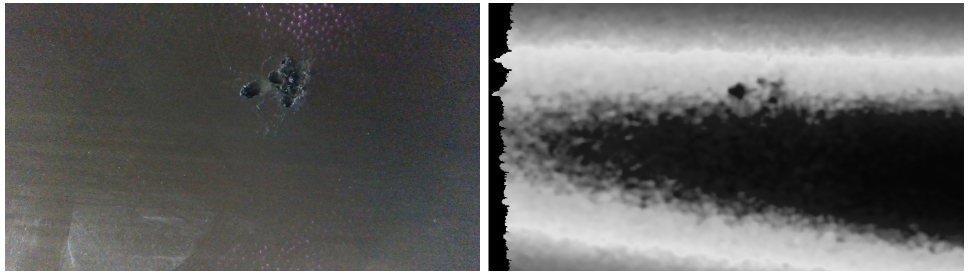

RGB-D data and Segmentation from a pipe sample

Depth Map Generation using D435i

Measuring the inherent noise level in the sensor:

$$\mathrm{R}MSE = \sqrt{z_i^2 - z_p^2}$$

The subpixel RMS error is given in the form of disparity in pixels and is a function of the plane-fit projected depth z_p and the actual depth z_i

What is the minimum change in depth the sensor can detect?

$$z = \frac{fb}{d}$$

$$dz = -\frac{z^2}{fb}dd + \frac{z}{b}db + \frac{z}{f}df$$

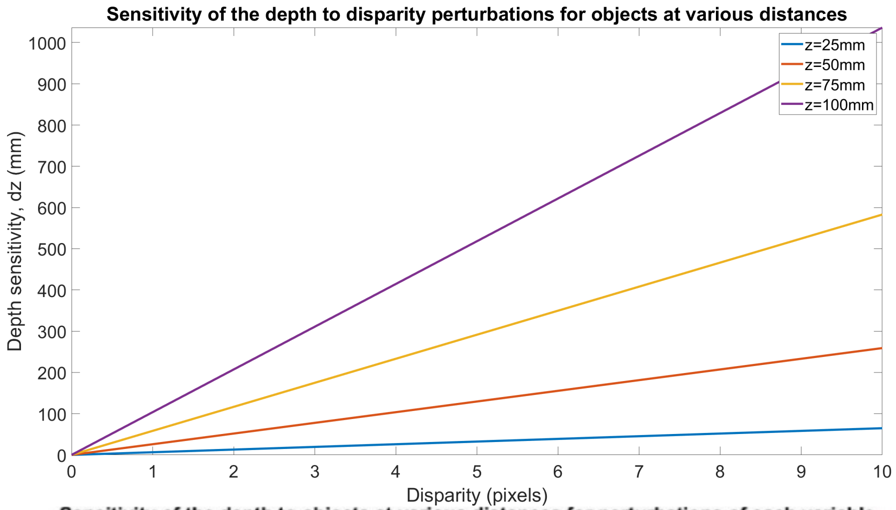

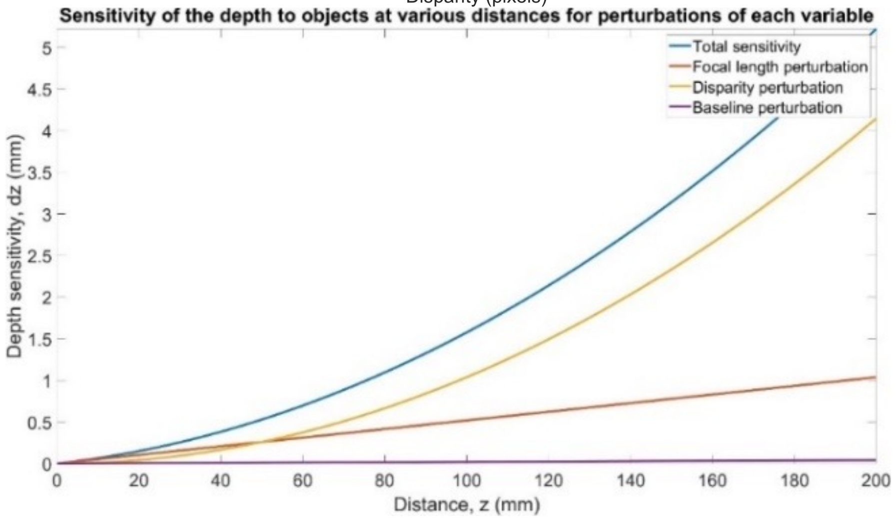

Depth Map Generation using D435i

Spatial Resolution : We use a pinhole camera model to convert image coordinate measurements into the corresponding world coordinate measurement, for a given resolution X_{res} and Y_{res}.

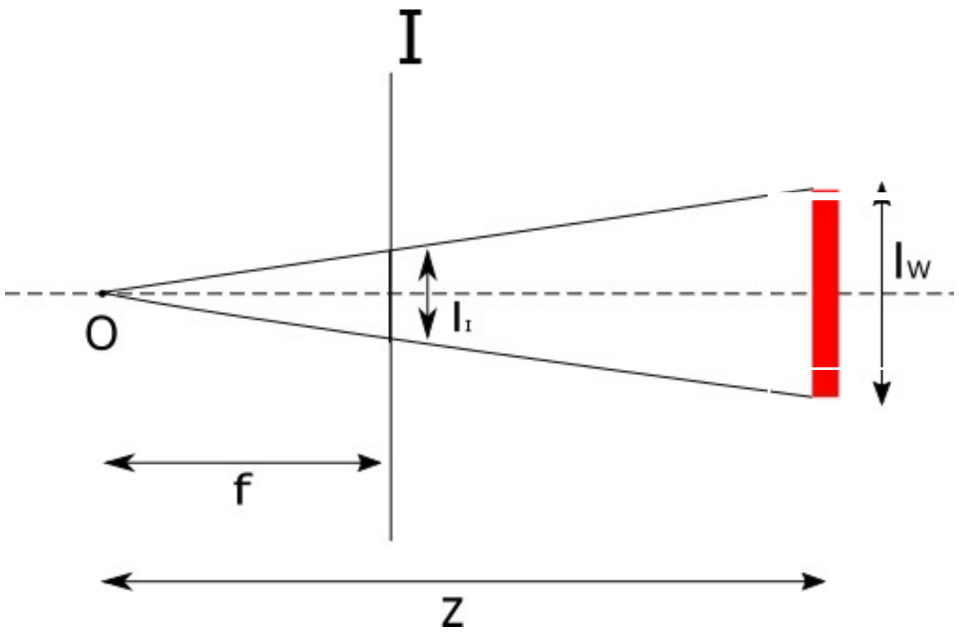

$$\frac{l_I}{f_x} = \frac{l_W}{z}$$

$$f_x = \frac{\frac{1}{2}X_{res}}{\tan\left(\frac{\theta_H}{2}\right)}$$

$$l_I = \frac{\frac{1}{2}X_{res}}{\tan\left(\frac{\theta_H}{2}\right)} \frac{l_w}{z}$$

Given the image resolution, focal length, depth and object length in the pixel space, you can compute the corresponding length in the world coordinate system.

For our case,

The D435i has a pixel size of 3μmx3μm. This gives us ~ 0.621 mm per pixel for an object that is 200mm away.

Depth Map Generation using D435i

SUMMARY of the empirical sensitivity analysis across key parameters for thickness and shape measurement using the D435i

Parameter	Min	Max	Summary of analysis findings	
			Thickness Error	Area Error
Exposure ($\frac{W}{m^2}s$)	0	70e5	BAND	BAND
Gain (dB)			FINE-TUNE	FINE-TUNE
Laser Power (W)	0	250	FINE-TUNE	FINE-TUNE
Second Peak Threshold (Px)	0	1000	↑ ↓	↑ ↑
Neighbor Threshold (Px)	0	500	↑ →	↑ ↑
Disparity Shift (Px)	0	175	BAND	BAND

Symbol	Meaning
BAND	Best values found in a band, beyond which errors grow.
FINE TUNE	Fine-tune along with or after exposure tuning.
↑ ↑ / ↑ ↓	Relation between parameter (blue) and error (red) variation.

Depth Map Post Processing Techniques

Hole Filling by Colorization

Classical Image Processing-based inpainting technique, originally used for colorizing monochrome images.

Encodes an implicit notion of continuity, weighted by RBF, to the depth map by minimizing the following function:

$$J(U) = \sum_{r} \left(I(r) - \sum_{s\, \epsilon N} w_{rs} I(s) \right)^2 \qquad w_{rs} = e^{-\frac{(I(r)-I(s))^2}{2\sigma_r^2}}$$

RGB

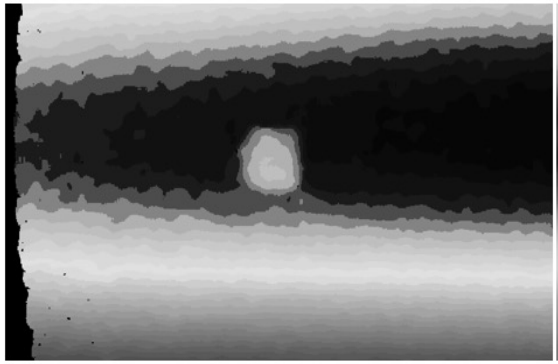

Unprocessed depth map

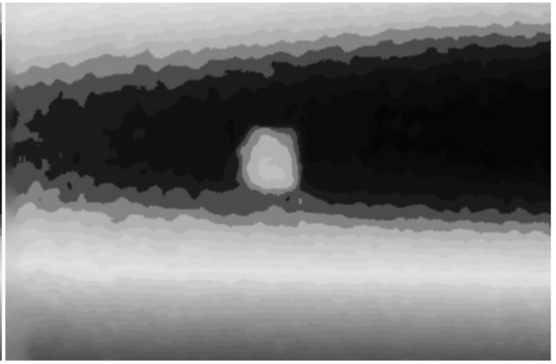

Processed depth map

Depth Map Post-Processing Techniques

Extremum Seeking Controller

Camera parameter fine-tuning using an Extremum Seeking Controller (ESC) to dynamically tune the map according to the following objective function:

$$J(x) = -\log\left(\frac{n_f}{WxH}\right)$$

n_f – pixels with valid depth values
W, H – Depth map dimensions

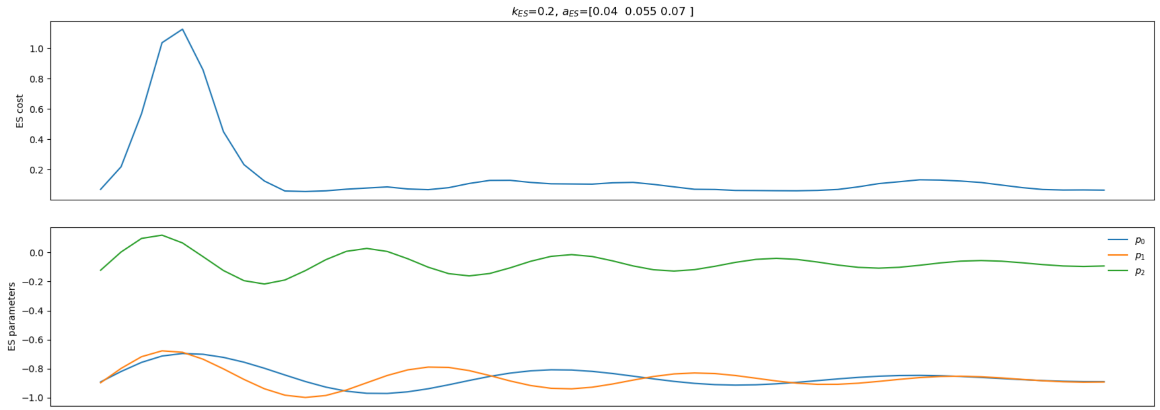

Cost function vs Iterations

Normalized parameter values vs Iterations

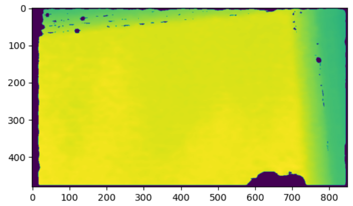

Final depth map

The plots show the evolution of the cost function and the parameters respectively.
The final solution for the depth map is shown in the figure.

Hardware Prototyping

INITIAL DESIGN

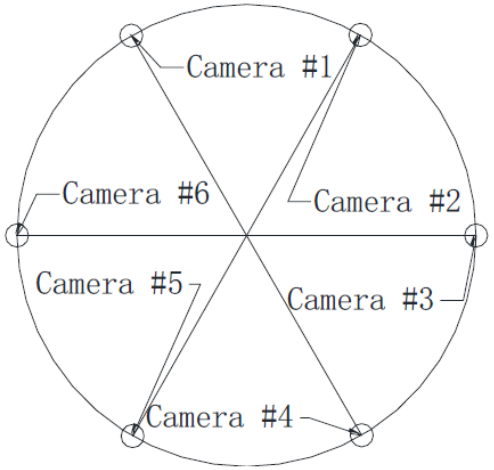

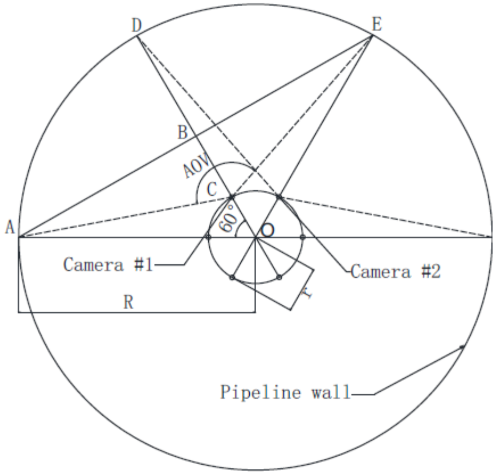

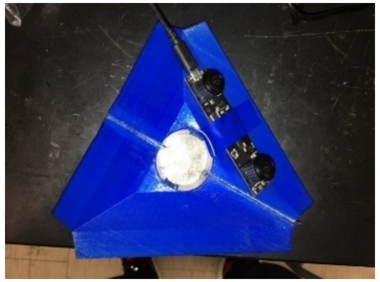

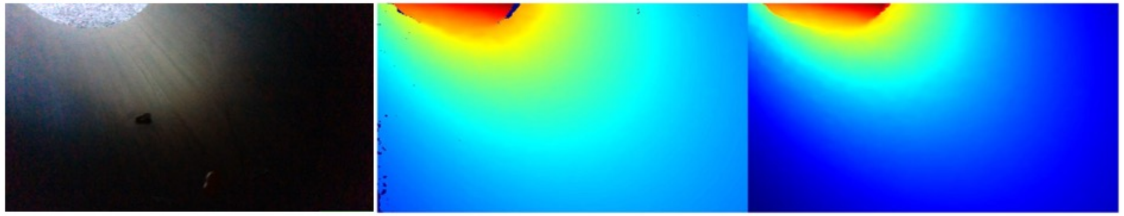

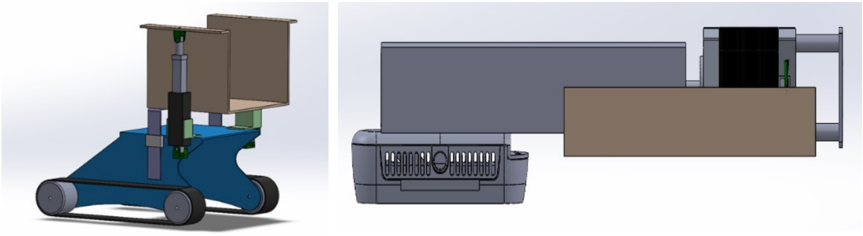

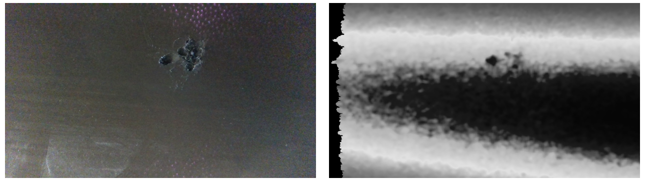

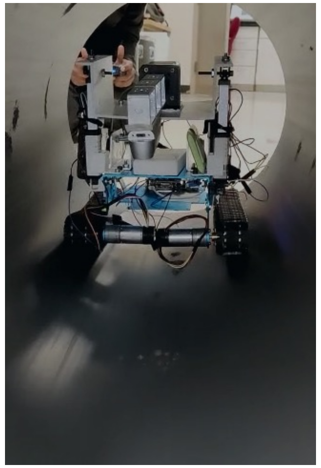

MODIFIED DESIGN

- Co-axiality of the stereo-camera with the pipe
- Orthogonality of the camera with the pipe surface
- 3D printable parts alongside standard mounts for motors.

Pipeline Surface Mapping and Odometry

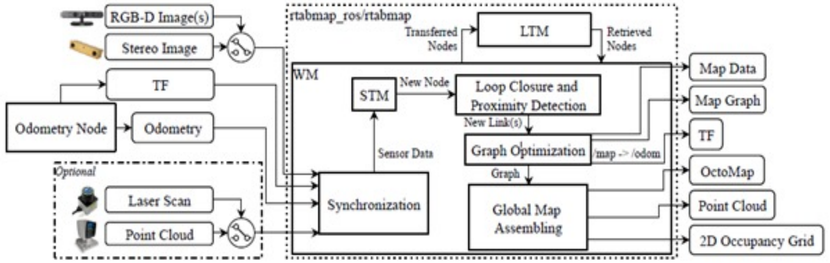

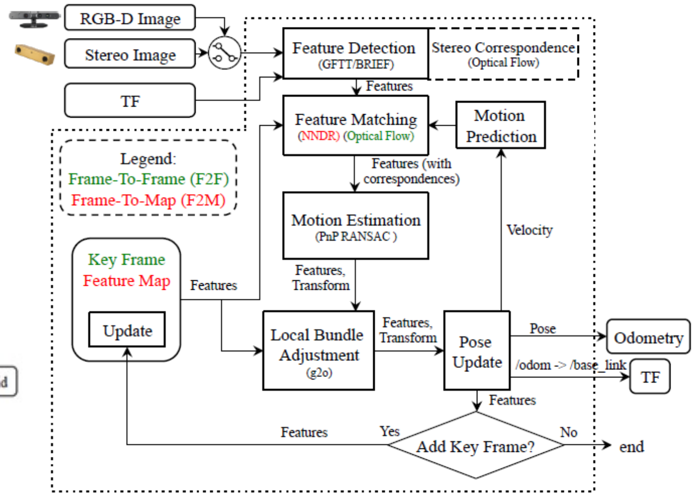

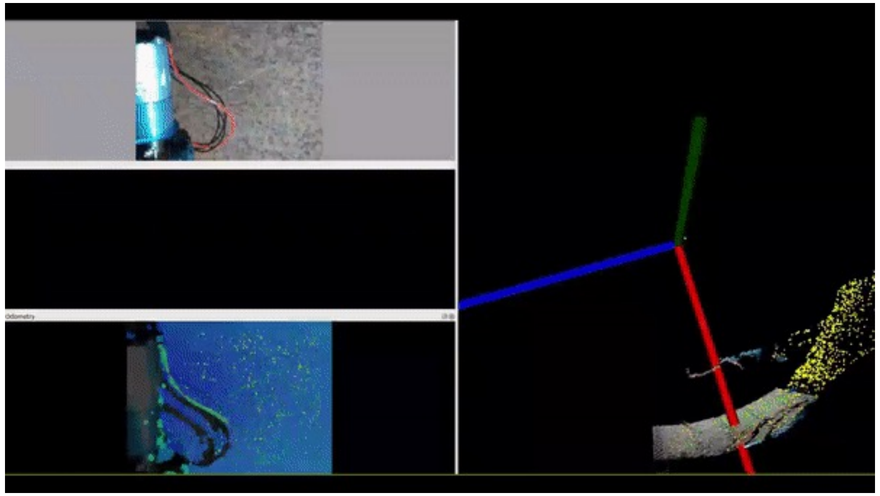

Pipe mapping demonstration (top) for a corroded metallic pipe. Pitch angle over time (bottom)

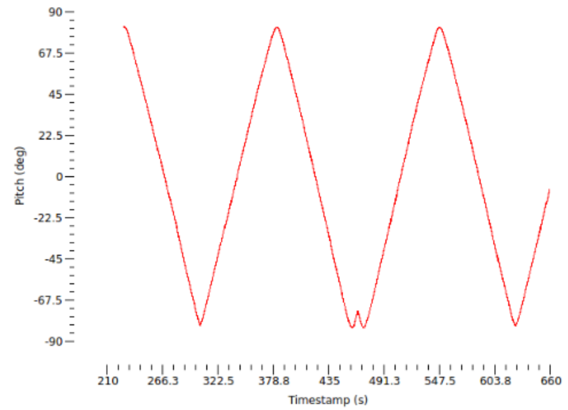

- RGB-D SLAM
  - Stitching and odometry during the scanning process.
  - Defect localization using IMU-Visual Odometry fusion.
  - SLAM works for arbitrary pipe shapes.

Pipeline Surface Mapping and Odometry

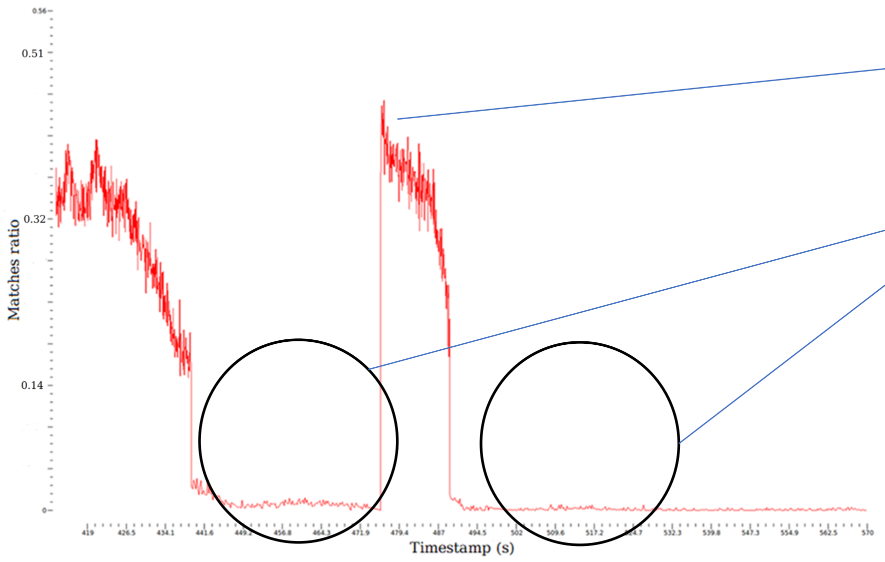

Feature match ratio peaks at ~ 0.4

Intermittent loss of matches leading to errors in image stitching

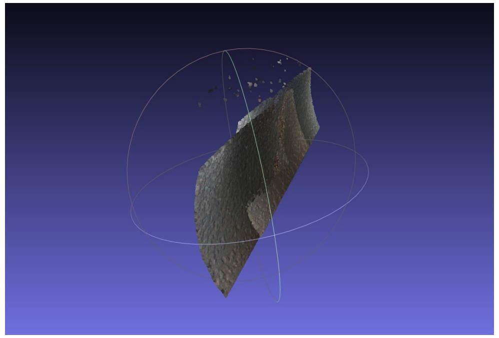

SLAM-based stitching with a low inlier ratio for features.

- Challenges:
  - Featureless surfaces can cause high uncertainty in robot position
  - Jerky odometry worsens reconstruction
- Potential solutions:
  - Using additional sensing elements (stepper motor data) to inform camera angle

Uncertainty Modeling

- Motivations:
  - How would predictions be impacted if there's not enough data?
  - How would predictions be impacted if the test data is different from what we trained on?
- **Classifiers** vs Regression models
- Epistemic vs Aleatoric uncertainty
  - Most types of uncertainty are "reducible".
  - Sources of uncertainty assumed "irreducible":
    - Sensor noise
    - Occlusion, reflections and other image artifacts

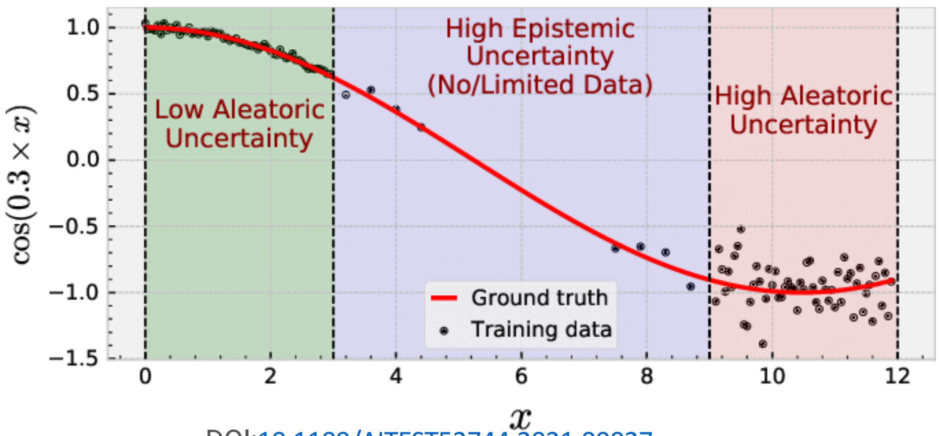

DOI:10.1109/AITEST52744.2021.00027
Uncertainty in regression

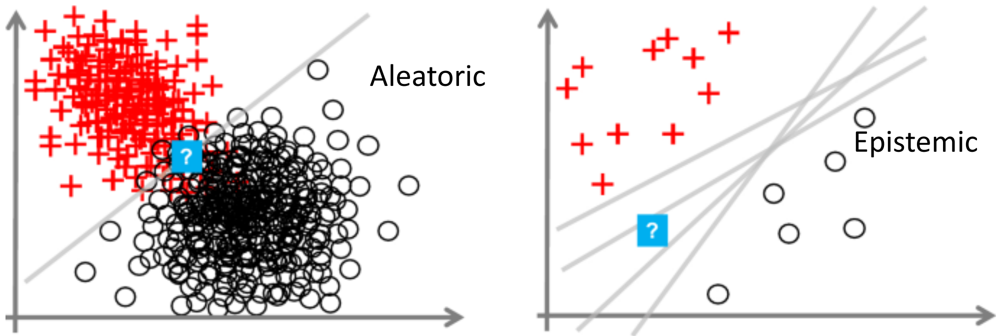

Uncertainty in classification
DOI: https://doi.org/10.1007/s10994-021-05946-3

Background – MC Dropout

Bayesian Inference:
Prior : $p(f)$ where f is a sample from the distribution of functions that could have generated the data

$$y = f(x), x \in X, y \in Y.$$

Likelihood : $p(Y|f, X)$.

Posterior : $p(f|Y, X) \propto p(Y|f, X)p(f)$

Posterior predictive for a new sample:

$$p(y^*|x^*, X, Y) = \int p(y^*|x^*, w)p(w|x^*, X, Y)dw$$

- **MC-Dropout FCN:**
  - A form of model averaging by changing model complexity randomly over multiple sampling iterations.
  - Key Idea: Modify the deep neural net by adding in a dropout layer and use the dropout layer during inference to randomly remove model parameters to get an averaged output from multiple models.

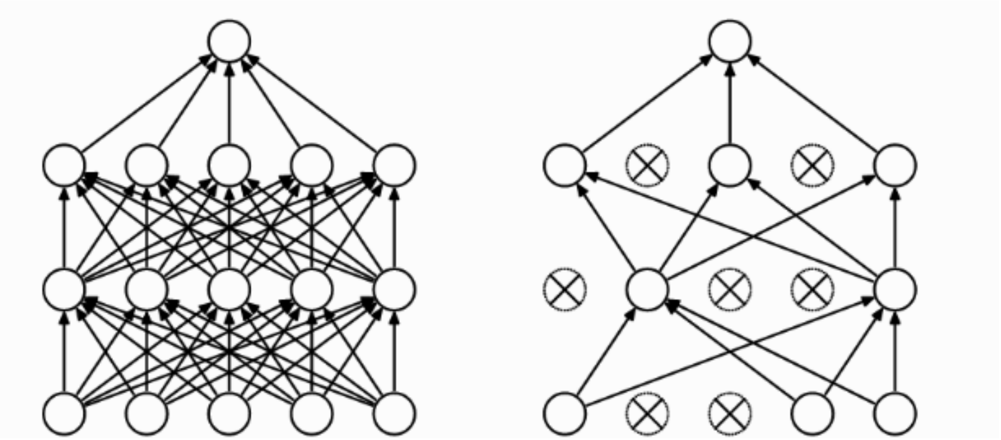

Illustration of dropout in neural nets*
(source: https://proceedings.mlr.press/v48/gal16.html)

Uncertainty Modeling for Classification using MC-Dropout

Classification

Assume binary training data generated from Bernoulli

$$y_i | x_i \sim Bern(\phi(w^T x_i))$$

$$\phi - softmax$$

$$w = argmax_w p(y_i | x_i, w)$$

This formulation leads to a stochastic negative log likelihood loss by first setting up a Gaussian distribution using the predicted mean and variances:

$$y_i | W \sim N(f(x)_i^w, \sigma^{w\,2}_{\,i})$$

$$p_i = \phi(y_i)$$

$$y_{i,t} = f(x_i)^W + \epsilon_t \; \epsilon_t \sim N(0,, \sigma^{w\,2}_{\,i})$$

$$L_x = NLL(y_{i,t}, y)$$

This is implemented by first transforming the $y_{i,t}$ using the log sum exp trick and passing it onto the NLL loss function.

Verification - Classification

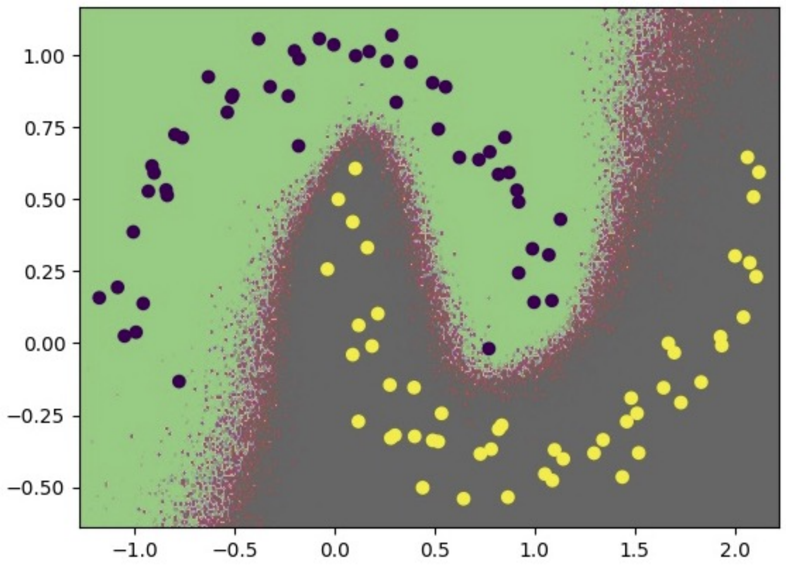

(a)

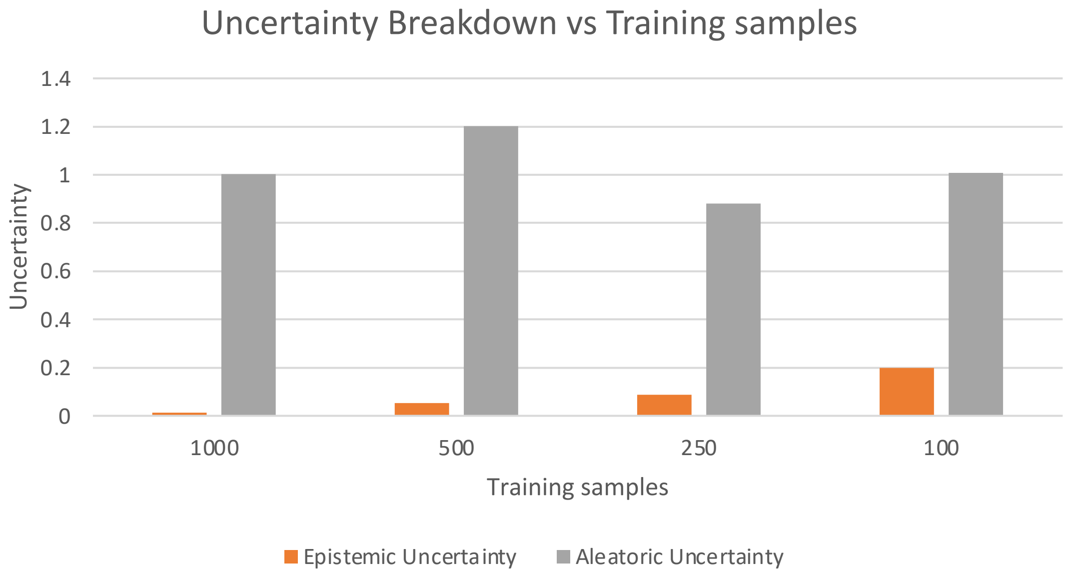

(b)

(a) Decision boundary for the two-moons classifier (b) Epistemic and aleatoric uncertainty across training samples

Depth-Normal-Curvature Representation

RGB-DNC representation

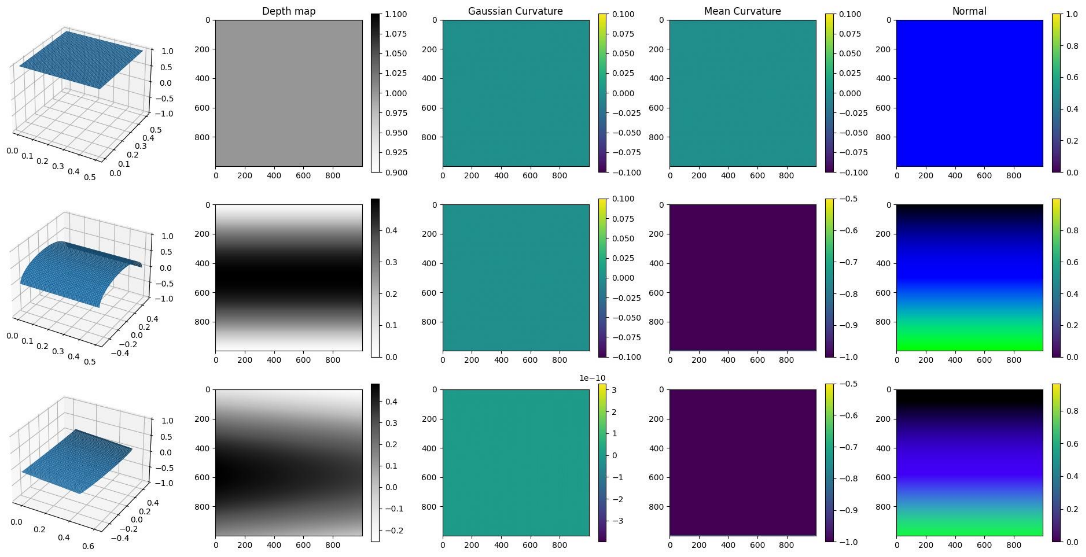

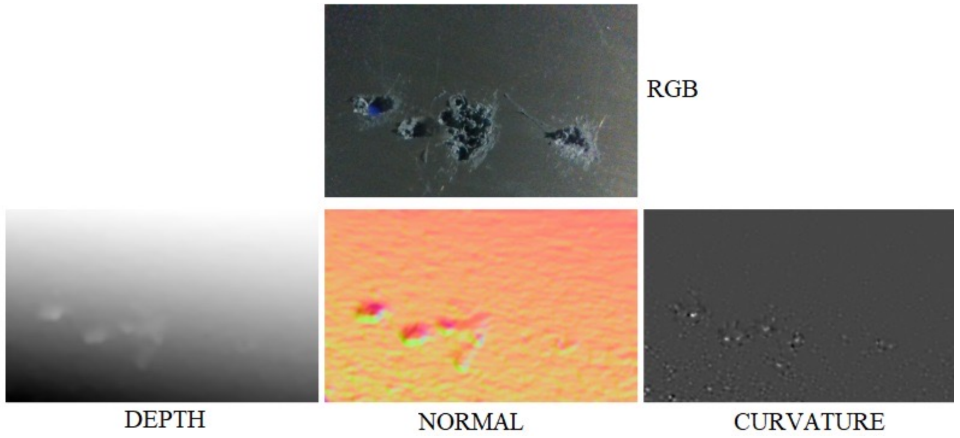

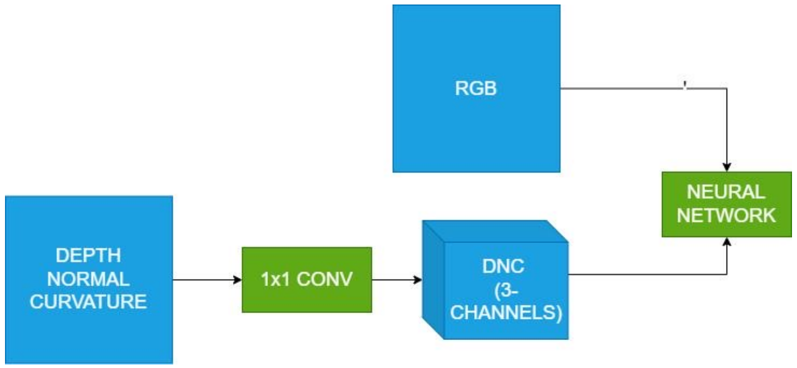

Uncertainty Quantification using MC-Dropout

Analysis on the ASU Pipe RGB-D Dataset

TrainSamples	DataFmt	MeanF1	Class0_F1	Class1_F1	Class2_F1
4	rgb	0.406	0.916	0.214	0.088
	rgbd	0.427	0.939	0.249	0.092
	rgbdc	**0.435**	0.956	**0.250**	0.098
	rgbdnc	0.433	**0.959**	0.239	**0.102**
9	rgb	0.420	0.941	0.209	0.109
	rgbd	0.434	**0.942**	**0.271**	0.088
	rgbdc	**0.438**	0.941	0.234	**0.139**
	rgbdnc	0.389	0.911	0.155	0.102
14	rgb	0.437	0.949	0.224	0.138
	rgbd	0.465	0.955	0.312	0.128
	rgbdc	**0.497**	**0.962**	**0.346**	**0.182**
	rgbdnc	0.470	**0.962**	0.313	0.136
19	rgb	0.386	0.912	0.137	0.108
	rgbd	0.415	0.923	0.238	0.083
	rgbdc	**0.479**	0.923	**0.370**	**0.144**
	rgbdnc	0.459	**0.950**	0.317	0.110

TrainSamples	DataFmt	MeanEpi	Class0_Epi	Class1_Epi	Class2_Epi
4	rgb	0.0059	0.0079	0.0048	0.0049
	rgbd	0.0053	0.0074	0.0044	0.0041
	rgbdc	0.0047	0.0067	**0.0030**	0.0044
	rgbdnc	**0.0041**	**0.0057**	**0.0030**	**0.0035**
9	rgb	0.0051	0.0071	0.0038	0.0044
	rgbd	0.0050	0.0071	0.0035	0.0044
	rgbdc	**0.0044**	**0.0062**	**0.0036**	**0.0034**
	rgbdnc	0.0056	0.0073	0.0048	0.0046
14	rgb	0.0040	0.0057	0.0030	0.0032
	rgbd	0.0043	0.0061	0.0031	0.0036
	rgbdc	0.0036	0.0051	0.0032	**0.0024**
	rgbdnc	**0.0034**	**0.0049**	**0.0026**	0.0027
19	rgb	0.0065	0.0089	**0.0045**	0.0062
	rgbd	0.0060	0.0080	0.0048	0.0051
	rgbdc	**0.0056**	**0.0076**	**0.0045**	**0.0047**
	rgbdnc	0.0059	0.0084	0.0039	0.0055

TrainSamples	DataFmt	MeanAle	Class0_Ale	Class1_Ale	Class2_Ale
4	rgb	1.000	1.000	**1.000**	1.000
	rgbd	**0.999**	1.002	1.006	**0.990**
	rgbdc	1.004	**0.994**	1.014	1.003
	rgbdnc	1.013	0.996	1.009	1.033
9	rgb	**1.000**	0.999	0.999	1.001
	rgbd	1.000	1.002	**1.006**	**0.990**
	rgbdc	1.003	**0.993**	1.014	1.003
	rgbdnc	1.014	0.996	1.010	1.035
14	rgb	**0.999**	0.997	**0.999**	1.000
	rgbd	1.000	1.006	1.008	**0.986**
	rgbdc	1.005	**0.991**	1.014	1.010
	rgbdnc	1.018	0.994	1.015	1.044
19	rgb	**0.999**	0.997	**0.999**	1.000
	rgbd	1.001	1.005	1.009	**0.989**
	rgbdc	1.007	**0.991**	1.014	1.016
	rgbdnc	1.020	0.993	1.019	1.049

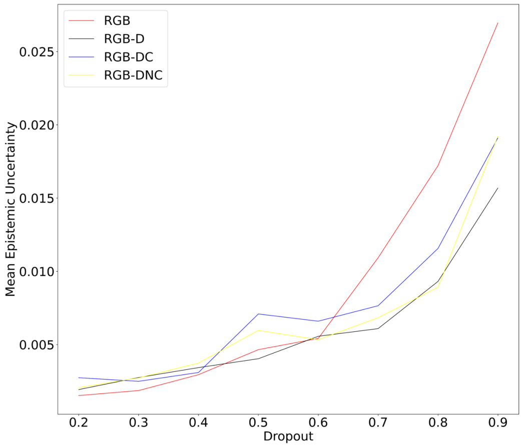

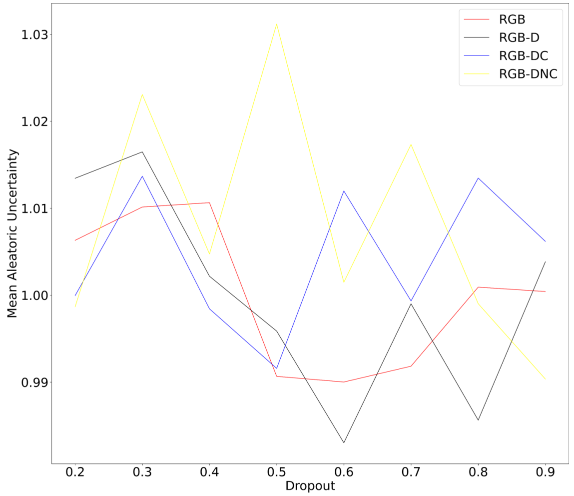

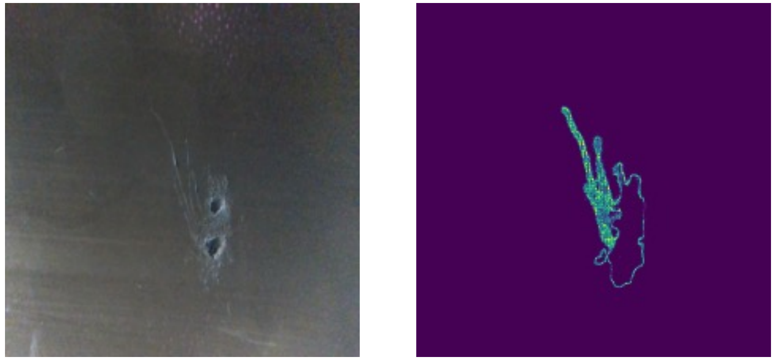

Most of the uncertainty is in the boundary of the defect

Uncertainty Quantification using MC-Dropout

Analysis on the ASU RGB-D Pipe Dataset – Calibration of the detections

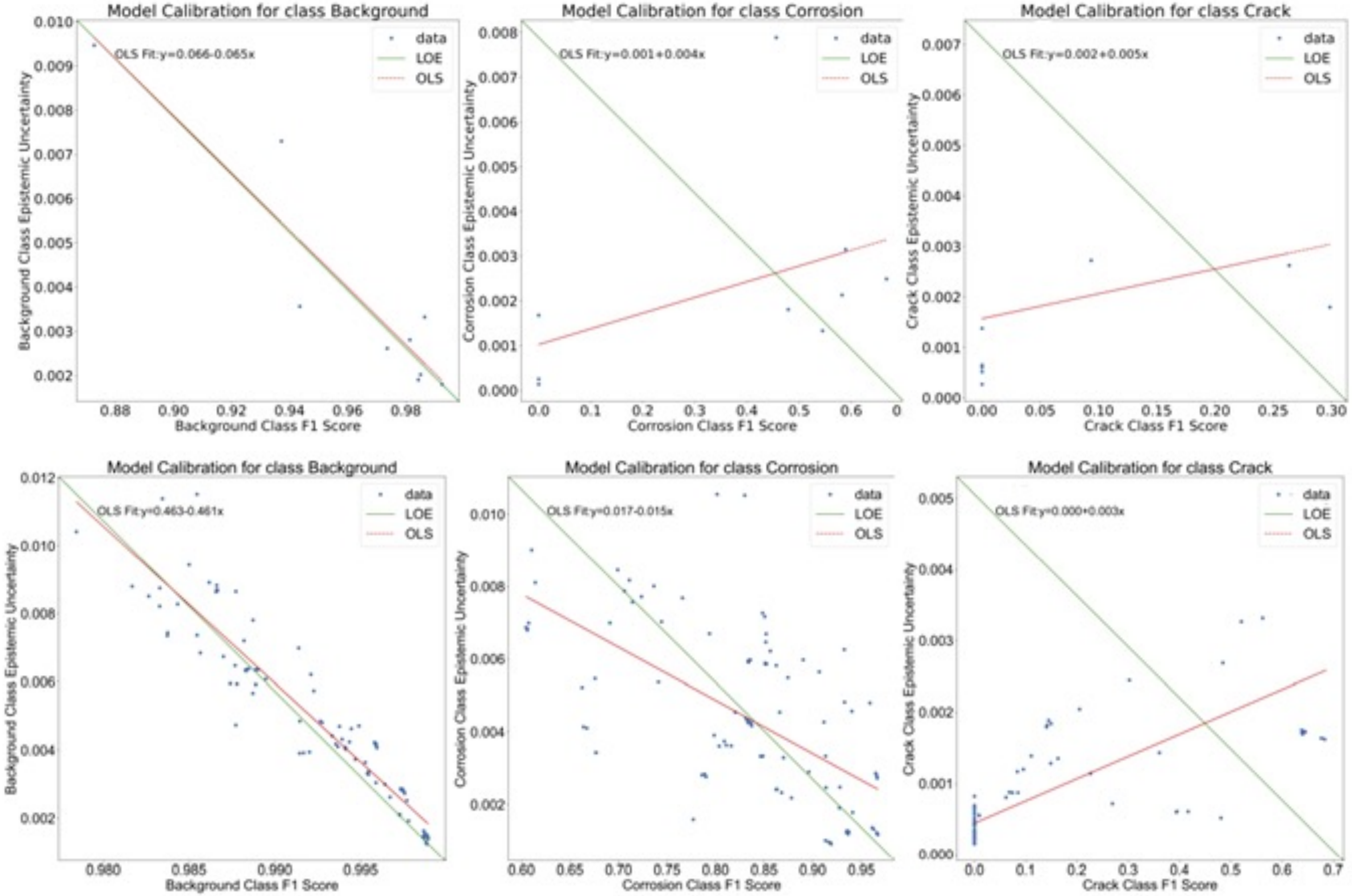

Small dataset

Larger, Augmented dataset

Uncertainty Quantification using MC-Dropout

Fusion-Method	DataFMT	mF1	Background F1	Corrosion F1	Crack F1
Element-wise Add	DNC	0.444	**0.962**	0.247	0.120
Recalibration Filter*	DNC	0.452	0.946	0.255	**0.138**
Ours	DNC	**0.459**	0.950	**0.317**	0.110

*Chen, Xiaokang, et al. "Bi-directional cross-modality feature propagation with separation-and-aggregation gate for RGB-D semantic segmentation." *European Conference on Computer Vision*. Springer, Cham, 2020.

Learning with Limited Data: Semi-Supervised Defect Localization using Activation Map Interpolation

- **Key idea:** Perturb inputs using augmentation to generate samples in the neighborhood of the original sample. Then, constrain the prediction of the neural network for both samples.

$$x_{mix} = a.T_1(x_1 + \epsilon_1) + (1 - a).T_2(x_2 + \epsilon_2)$$
$$y_{mix} \approx a.T_1(y_1 + \epsilon_1) + (1 - a).T_2(y_2 + \epsilon_2)$$

- T_i are image transformations and ϵ_i is a noise function.

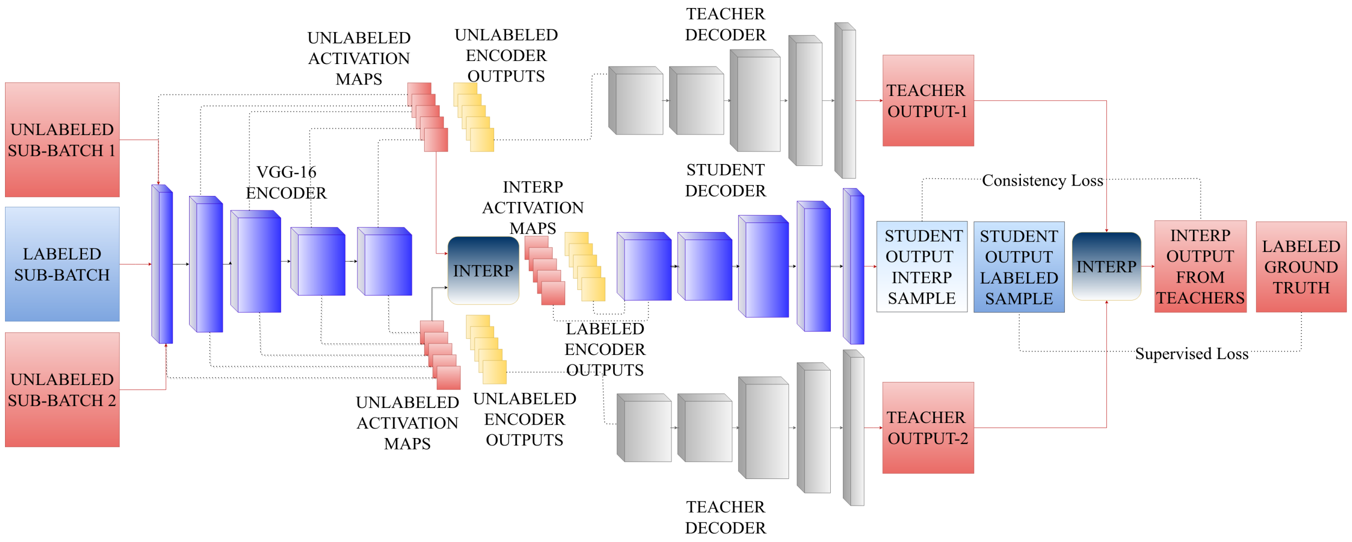

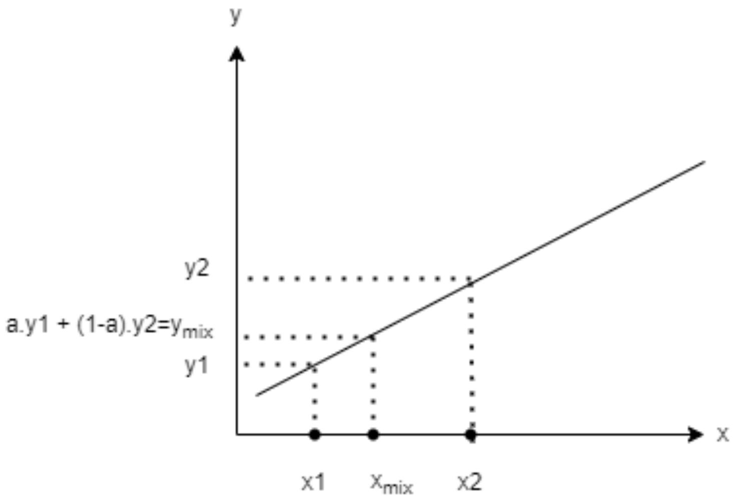

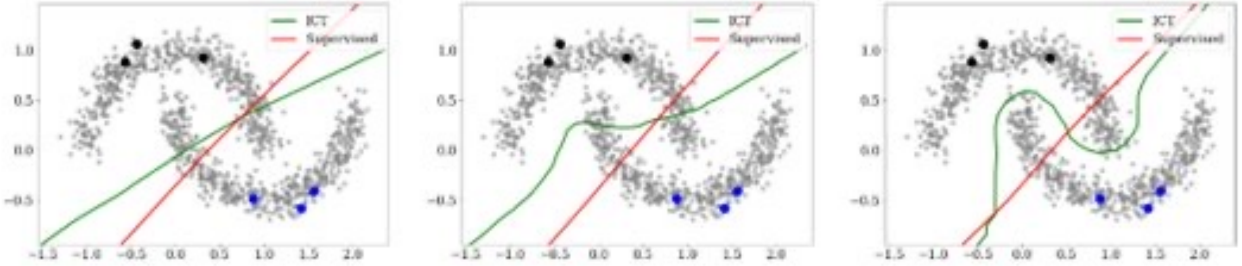

Semi-supervised learning using ICT: Latent information from unlabeled data can be leveraged using supervision from a limited training set. Overall approach for segmentation inspired from ICT

Image source: https://doi.org/10.24963/ijcai.2019/504

Semi-Supervised Defect Localization using Activation Map Interpolation

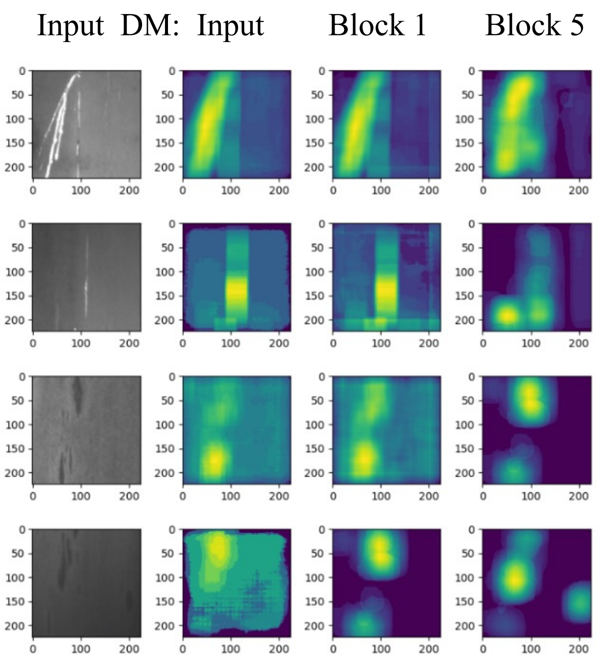

Cluster assumption demonstration by computing the patch wise Euclidean distance between a patch and its neighbors

- The *cluster assumption* is a key concept that we use to justify why we perform interpolation in the latent space.
- *Consistency regularization* constrains the predictions in the neighborhood of a sample to produce the same prediction as the unperturbed sample and is based on the validity of the cluster assumption.

Dataset	Training	Validation
NEU	600	300
CrackForest	135	16

Demonstrative Results – NEU Surface Defects Dataset

Labeled samples	Supervision	mIU
0%	Consistency Loss Only	0.08
5%	Supervised	0.39
	Semi-Supervised	0.64
10%	Supervised	0.43
	Semi-Supervised	0.66
20%	Supervised	0.51
	Semi-Supervised	0.64
50%	Supervised	0.68
	Semi-Supervised	0.69
100%	Supervised	0.84

Method	Type	Labeled	mIU
SegNet [3]	Fully Supervised	100%	0.5657
PSPNet [29]	Fully Supervised	100%	0.7225
PGA-Net [7]	Fully Supervised	100%	0.8215
Ours	Fully Supervised	100%	0.8309
Ours	Semi-Supervised	5%	0.6429
Ours	Semi-Supervised	10%	0.6674
Ours	Semi-Supervised	20%	0.6454
Ours	Semi-Supervised	50%	0.6992

$$IOU = \frac{\text{area of overlap}}{\text{area of union}} =$$

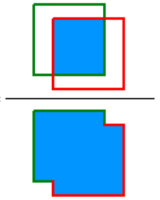

NEU Dataset:

3 defect types, 600 training images in total.

Performance metric:

mIU- mean (over # of classes) Intersection over Union

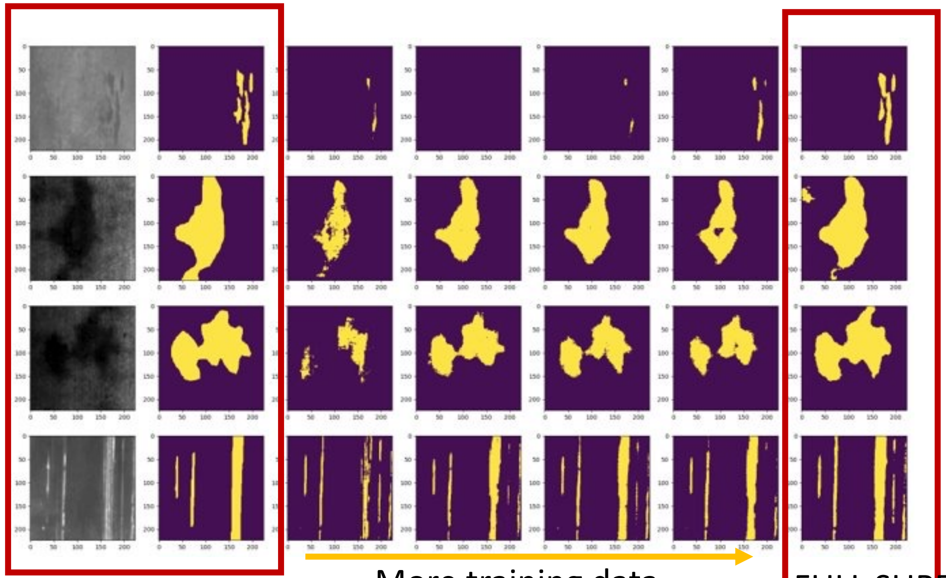

Demonstrative Results – Crack Defects Dataset

Method	Type	Labeled	Tolerance (px)	mIU	F-1
Canny	Image Processing	-	5	-	0.1576
CrackForest	Image-level labels + Hand engineered features	-	5	-	0.8571
U-Net	Fully Supervised	100%	0	0.55	0.7015
Res U-Net + ASPP	Fully Supervised	100%	0	0.56	0.7121
Ours	Fully Supervised	100%	0	0.7312	0.8443
Ours	Semi Supervised	5%	0	0.6944	0.8194
Ours	Semi Supervised	10%	0	0.6881	0.8151
Ours	Semi Supervised	20%	0	0.7109	0.8310
Ours	Semi Supervised	50%	0	0.6733	0.8047

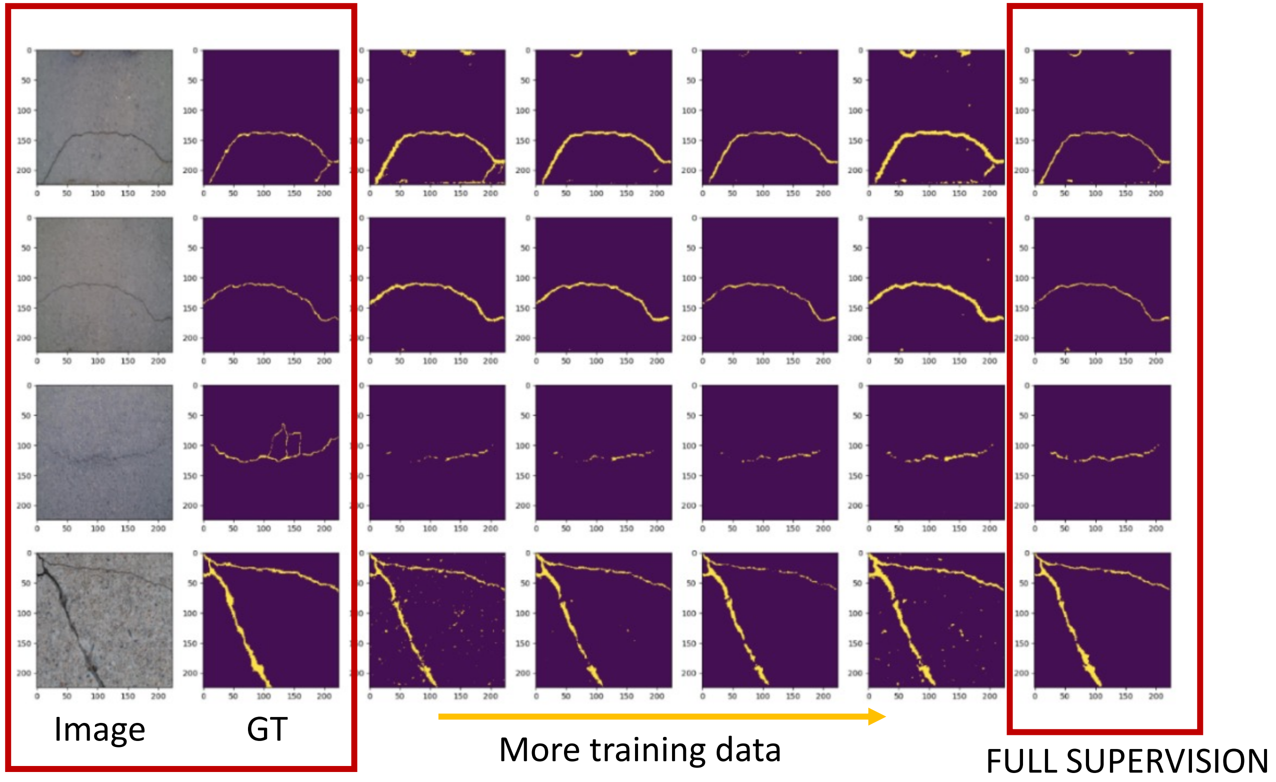

Demonstrative detections on the CrackForest validation set: (Left to Right) Image, Ground Truth, 5% Labeled, 10% Labeled, 20% Labeled, 50% Labeled, Fully Labeled

Post-Processing and Defect Characterization

Defect measurement after segmentation using point-cloud data

ASME B31G to estimate failure pressure using the measurements

FEM to estimate failure pressure using point-cloud data

Post Processing – Defect Measurement

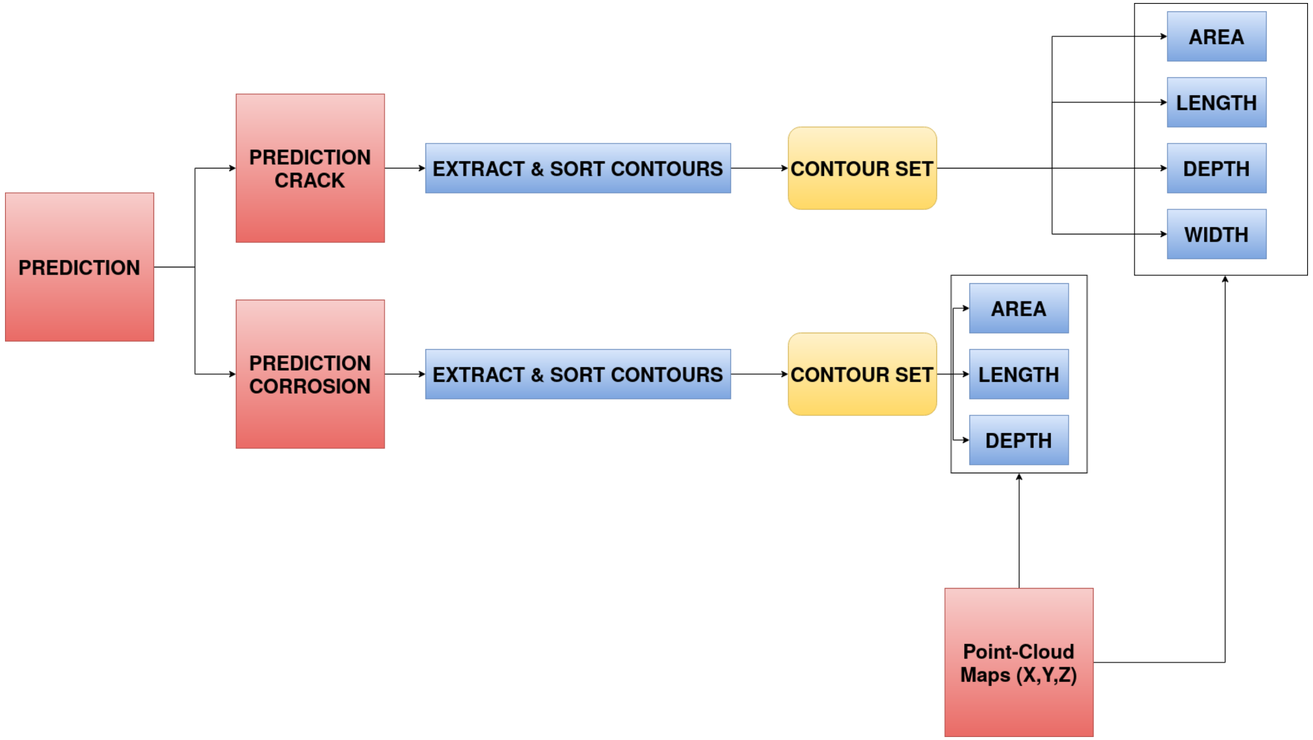

Image	Prediction	Defect	Measurement	From Prediction - Mean (SD)	From Ground Truth
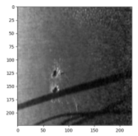	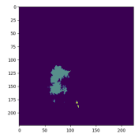	Pitting	Area (mm^2)	1577.47(74.56)	1028.01
			Depth(mm)	4.93(0.09)	4.79
			Length(mm)	44.98(0.84)	37.74
		Crack	Area(mm^2)	-	732.79
			Depth(mm)	-	2.4
			Length(mm)	-	57.24
			Width(mm)	-	7.9
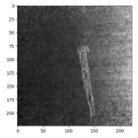	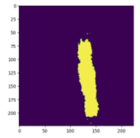	Crack	Area(mm^2)	3660.01(29.20)	2353.41
			Depth(mm)	2.11(4.23)	0
			Length(mm)	86.73(1.54)	79.92
			Width(mm)	23.02(0.28)	17.05

ASME B31G for modeling isolated defects

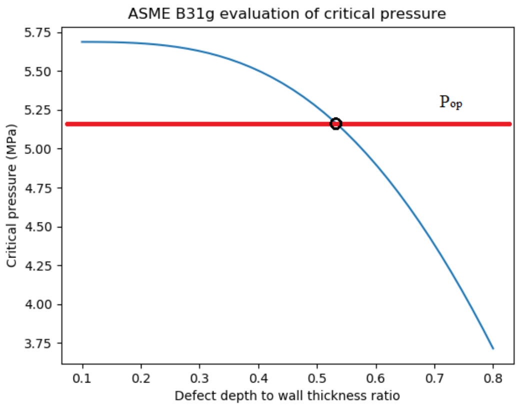

Prediction of failure pressure with depth to wall thickness ratio for a carbon steel pipe

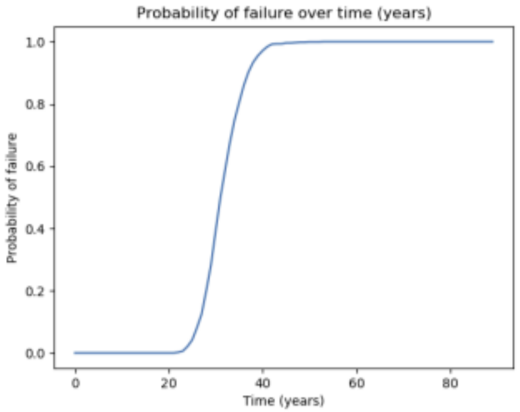

Probability of failure over time

Conventional technique of using ASME B31G standard has been used to model failure pressure

$$P_f = \frac{1.1 S_y 2t}{D}\left(\frac{1 - 0.85\left(\frac{d}{t}\right)}{1 - \frac{0.85\left(\frac{d}{t}\right)}{M1}}\right)$$

$$M1 = \sqrt{1 + 0.6275z - 0.003375z^2}\,, \qquad z = \frac{L^2}{Dt} \leq 50$$

$$M1 = 0.032z + 3.3, \qquad z = \frac{L^2}{Dt} > 50$$

We demonstrate failure pressure prediction based on an assumed rate of defect growth, for a single corrosion pit

$$\delta d \sim N_{\delta d}(\mu_{\delta d} = 0.1, \sigma_{\delta d} = 0.01)$$

$$\delta l \sim N_{\delta l}(\mu_{\delta l} = 0.1, \sigma_{\delta d} = 0.01)$$

$$s = P_f - P_{op} \; - Limit\ State$$

Extending to multiple corrosion pits requires additional models (FEA and FEA-based surrogates).

ASME B31g VS FEA for Interactive Threats

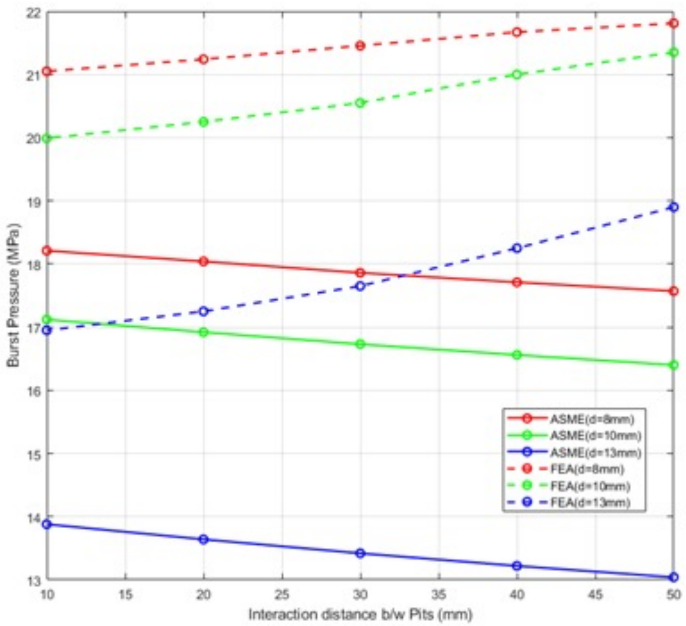

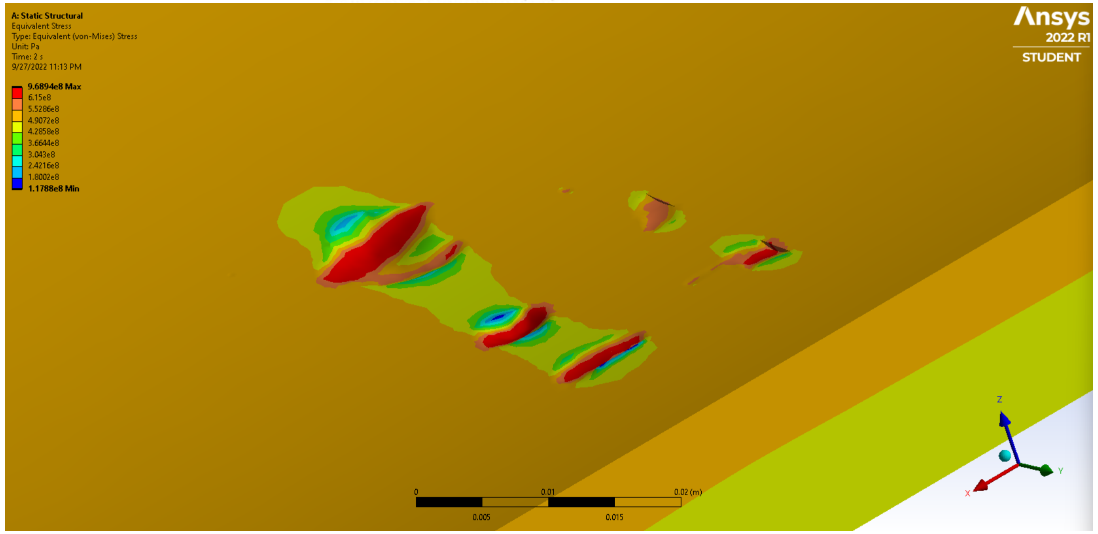

- The FEA analysis was performed for the pipeline with two interactive threats and validated against the experimental burst Pressure.
- The Parametric study was performed for the pipe with two interactive threats having 100mm length, 50mm width, and three different depths, i.e., 8, 10, and 13mm.
- The distance between two defects was varied, and FEA was used to predict the burst pressure
- ASME B31G does not consider pit interaction effects, but the FEM model does: This leads to a reduction in failure pressure point as the pits get closer.
- The point cloud data was used to create the pipe model with the actual surface and utilized FEA to evaluate the burst pressure.

Hardware-Software Integrated Prototype

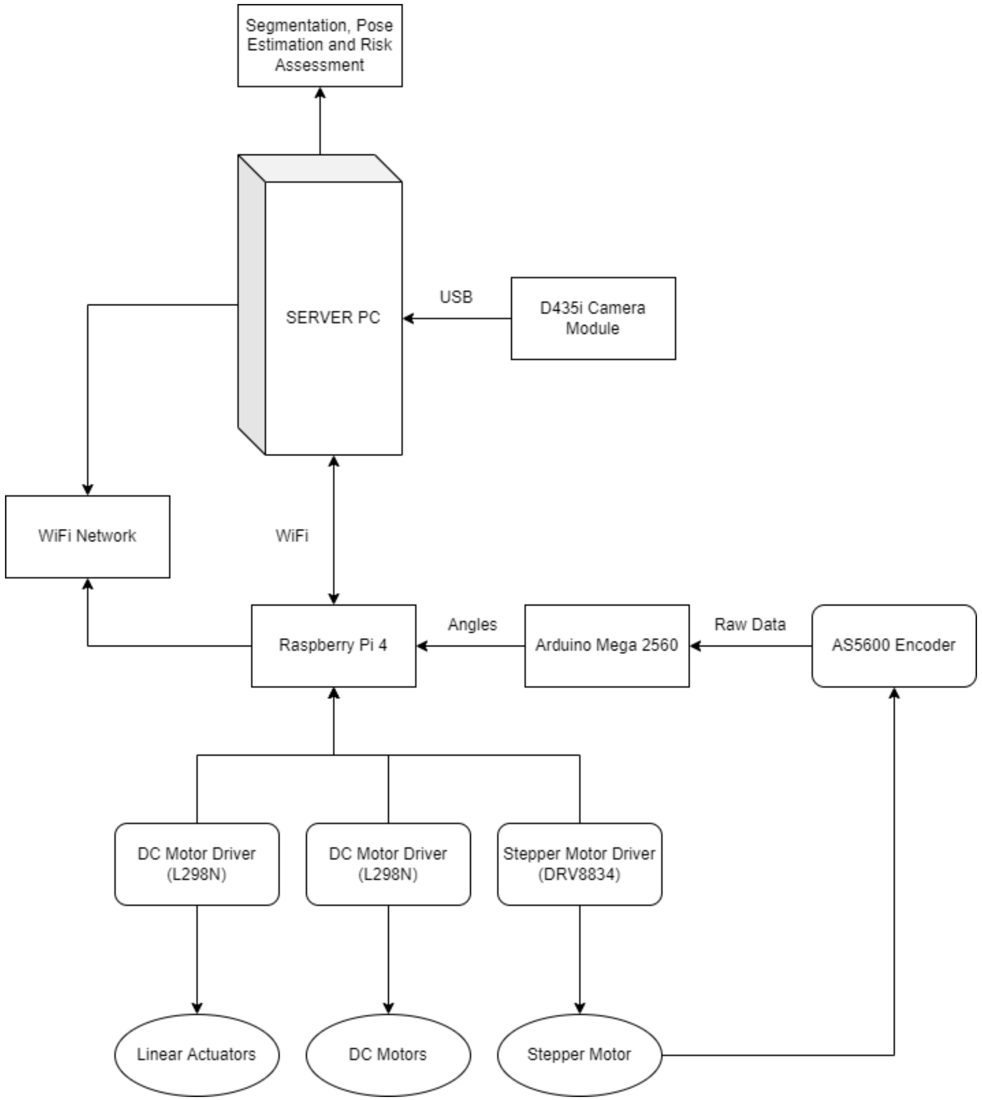

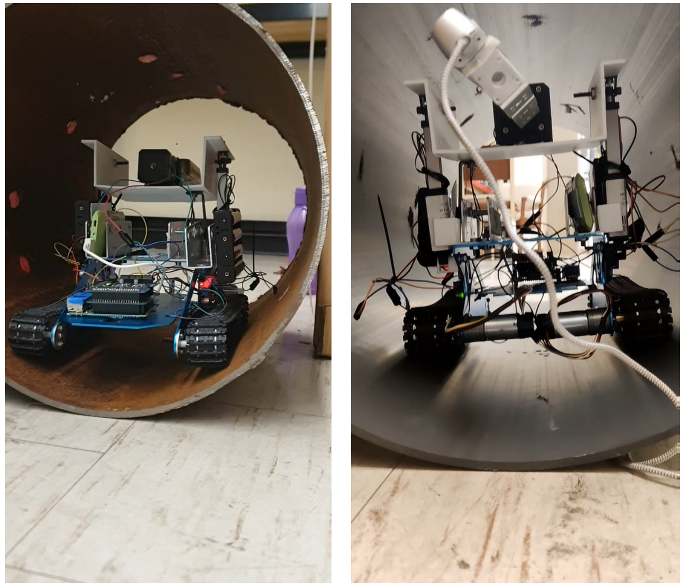

Robot Operation Demonstrations

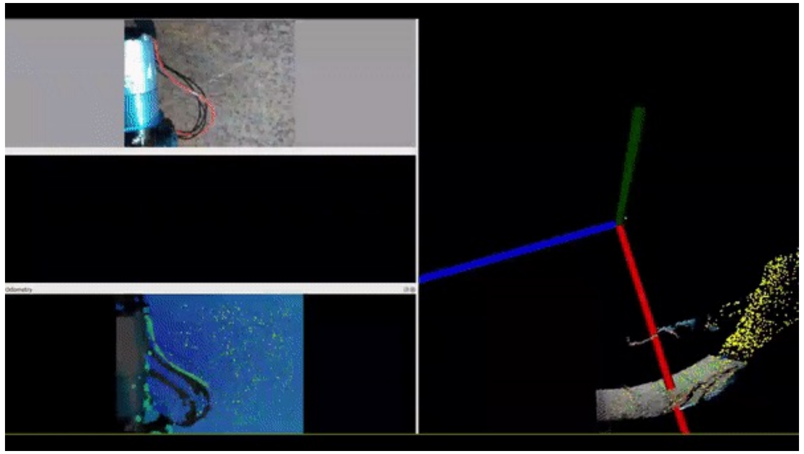

RTAB-Map RGB-D SLAM Mapping Demonstration

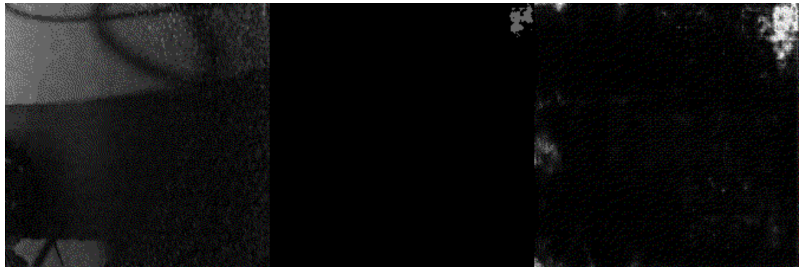

Image, Prediction: Mean and Variance

Conclusions

- Evaluation of a commercially available stereo-sensor for ILI
  - Millimeter scale depth and submillimeter scale spatial resolution can be achieved for corrosion defect detection.
  - Order of magnitude improvement in depth resolution is needed to make early failure prediction for defects such as narrow cracks.
- Fully supervised segmentation network with heteroscedastic uncertainty modeling
  - Semantic segmentation models have been developed to perform fine-grained localization of defects.
  - Uncertainty formulation can aid inspection protocols by providing indicators of distribution shift and lack of training data.
  - We predict aleatoric uncertainty along with a sampling-based method for epistemic uncertainty.
  - Results indicate that using additional depth and point cloud-derived surface maps such as normals and curvatures reduces model uncertainty and improves F-1 score.
- Semi supervised segmentation using activation map interpolation
  - Activation map interpolations are demonstrated to better obey the cluster assumption, enabling better representation clustering at the latent variable level, rather than at the input level.
  - Proposed method achieves up to 76% of the performance of a fully supervised model, using only 5% of the labeled data, on a large defect segmentation dataset.

Conclusions

- Models for defect post processing and risk assessment
  - Defect measurements using point cloud and segmentation results are used in the ASME B31G model for remaining life prediction
  - Improvements to the ASME B31G model using an FEM based model were proposed considering threat interactions
  - Based on the developed FEM model, our results indicate that using FEM-derived surrogates can account for interacting effects between multiple pitting defects, yielding more accurate failure estimates.
- Hardware-Software Integrated Prototype
  - Prototype hardware development using off the shelf equipment was performed
  - Developed ILI robot was deployed in pipe sample alongside the SLAM model and machine learning model to predict odometry and defect characteristics respectively.
  - Based on our experiments, we conclude that RGB-D SLAM is able to map corroded pipe surfaces. However, mapping feature-sparse surfaces requires additional investigation.

Next Steps

- Improving depth resolution for better detection of narrow crack depths
  - High resolution optical sensing
  - Stereo sensors fused with other modalities such as polarization sensing
- On-board odometry improvements in feature-sparse environments

Selected References

Gal, Yarin, and Zoubin Ghahramani. "Dropout as a bayesian approximation: Representing model uncertainty in deep learning." *international conference on machine learning*. PMLR, 2016.

Kendall, Alex, and Yarin Gal. "What uncertainties do we need in bayesian deep learning for computer vision?." *Advances in neural information processing systems* 30 (2017).

Ariyur, Kartik B., and Miroslav Krstic. *Real-time optimization by extremum-seeking control*. John Wiley & Sons, 2003.

Scheinker, Alexander, En-Chuan Huang, and Charles Taylor. "Extremum Seeking-Based Control System for Particle Accelerator Beam Loss Minimization." *IEEE Transactions on Control Systems Technology* 30.5 (2021): 2261-2268.

Verma, Vikas, et al. "Interpolation consistency training for semi-supervised learning." *Neural Networks* 145 (2022): 90-106.

French, Geoff, et al. "Semi-supervised semantic segmentation needs strong, varied perturbations." *arXiv preprint arXiv:1906.01916* (2019).

Labbé, Mathieu, and François Michaud. "RTAB-Map as an open-source lidar and visual simultaneous localization and mapping library for large-scale and long-term online operation." *Journal of Field Robotics* 36.2 (2019): 416-446.

Thank you for your attention. Questions?

CONTACT INFORMATION
Dr. Yongming Liu
ENGRC 409
Engineering Research Center
Tempe, AZ 85287-6106
Mailcode: 6106
Phone 480-965-6883
Email yongming.liu@asu.edu
Google Scholar

Project Details

Public page for more details on the project

[Research & Development Program: AI-enabled Interactive Threats Detection using a Multi-camera Stereo Vision System (dot.gov)]